Applied Catalysis B: Environmental 163 (2015) 167–178

Contents lists available at ScienceDirect

Applied Catalysis B: Environmental

journal homepage: www.elsevier.com/locate/apcatb

Direct formic acid fuel cells on Pd catalysts supported on hybrid TiO_2-C materials

Juan Matos[a,*], Andrzej Borodzinski[b,**], Anna Mikolajczuk Zychora[b], Piotr Kedzierzawski[b], Bogusław Mierzwa[b], Karol Juchniewicz[b], Marta Mazurkiewicz[c], Juan C. Hernández-Garrido[d]

[a] Department of Photocatalysis and Alternative Energies, Venezuelan Institute for Scientific Research (IVIC), 20632, Caracas 1020-A, Venezuela
[b] Institute of Physical Chemistry, Polish Academy of Sciences, Kasprzaka 44/52, 01-224 Warsaw, Poland
[c] Faculty of Materials Science and Engineering, Warsaw University of Technology, 02-507 Warsaw, Poland
[d] Departamento de Ciencia de los Materiales e Ingeniería Metalúrgica y Química Inorgánica, Facultad de Ciencias, Universidad de Cádiz, Campus Rio San Pedro, Puerto Real, 11510 Cádiz, Spain

ARTICLE INFO

Article history:
Received 27 March 2014
Received in revised form 22 June 2014
Accepted 29 July 2014
Available online 7 August 2014

Keywords:
Fuel cells
Formic acid
Pd-based catalysts
TiO_2-C hybrids

ABSTRACT

The electrooxidation of formic acid was performed on Pd-based catalysts supported on hybrid TiO_2-C materials prepared from different carbon origins by solvothermal and slurry synthesis. It has been found that carbonized hybrid TiO_2-C supports with mesopore texture and high anatase:rutile ratio in the TiO_2 framework led to about three times higher activity per Pd mass unit than the catalyst prepared on a commercial Vulcan XC-72 carbon black, which will allow to reduce considerably the amount of expensive noble metal at the anode of DFAFC. The conductivities of raw TiO_2/C supports are several orders of magnitude lower than that for carbon Vulcan XC-72. However, the hybrid TiO_2-C supports acquire high conductivity during palladium deposition. The rate of electrooxidation of formic acid on Pd/TiO_2-C catalysts, calculated per one surface Pd atom (TOF), is for TOF < 1 s^{-1} independent of Pd particle size and morphology of the supports. Higher activity of the Pd/TiO_2-C catalysts, compared to Pd/C catalyst, results from their higher hydrophilicity which ensures good access of formic acid to the Pd crystallites in the catalyst layer, and sufficiently high conductivity providing easy electron flow from the Pd active sites to current collector. Present results indicate that hybrid inorganic/organic materials are promising supports for the direct formic acid fuel cells with Pd-based catalysts.

1. Introduction

One of the most important challenges for science is the direct conversion of chemical energy in electricity via a fuel cell. Hydrogen is often seen as a likely fuel for fuel cells because its oxidation is mechanistically the easiest. However, H_2/O_2 fuel cell requires either on-site H_2 storage or an on-board reformer to extract H_2 from organic fuels [1]. Thus, the oxidation of small organic molecules such as methanol, ethanol or formic acid is an attractive alternative for the direct fuel cells [2–12]. Formic acid has been attracting a great attention as a promising alternative fuel [2–5,10,11,13–20] for the so-called direct formic acid fuel cells (DFAFC). The advances in DFAFC have been reviewed recently [17] and it has the following advantages [11,17]: (i) higher power density, higher energy efficiency and higher electromotive force than methanol fuel cell, (ii) formic acid as a liquid is easy to handle, (iii) crossover flux of formic acid through Nafion membrane is several times smaller than that of methanol [21], (iv) formic acid is less toxic than methanol and does not have the risk of producing hazardous by-products during oxidation (e.g. formaldehyde), (v) it allows using highly concentrated fuel solution (up to 15 M compared to only 3 M for methanol), (vi) palladium alloys used as catalysts in DFAFC are cheaper and have better availability than platinum ones. The main drawback of formic acid as a fuel is its low energy density; however it is compensated by the high-energy efficiency of DFAFC. In addition, a direct fuel cell requires the use of a catalyst supported on materials with specific properties. The ideal support material for fuel cell electrocatalysts should have the following characteristics [12]: high electrical conductivity, good mechanical properties, high specific surface area, adequate water-handling capability at

* Corresponding author. Tel.: +58 2125041166; fax: +58 2125041166.
** Corresponding author.
E-mail addresses: jmatos@ivic.gob.ve, jmatoslale@gmail.com (J. Matos), aborodzinski@ichf.edu.pl (A. Borodzinski).

http://dx.doi.org/10.1016/j.apcatb.2014.07.063
0926-3373/

the electrode and also good corrosion resistance under oxidizing conditions. Carbon is an ideal candidate as the support material for fuel cell electrocatalytic applications. Besides conventional carbon anodes [7,8], new carbon materials such as carbon nanotubes [22] and hybrid metal oxides/carbon nanocomposites have attracted interest as supports for electrocatalysis [10,12] and oxidation reactions [23]. In addition, hybrid materials constituted by carbon and metal oxides such as WO_3 [5,6,10] are stable in acid solutions being an advantage to support Pd or Pt electrocatalysts because hydrogen can spill-over onto the surface of WO_3 by the formation of hydrogen tungsten bronze, freeing noble metal sites for further chemisorption of hydrogen from the liquid fuels and improving support conductivity. In the present work Pd-based catalysts supported on hybrid TiO_2-C materials were prepared by solvothermal synthesis followed by Pd deposition on such supports. There are several reasons for choosing of TiO_2 addition to carbon support for the Pd catalysts of formic acid electrooxidation: (i) TiO_2 addition to Pt/carbon catalysts had a positive effect in electroxidation of hydrogen [24]; (ii) it was shown that anode catalyst layer for formic acid electrooxidation should be hydrophilic [25,26] and it was expected that TiO_2 addition would increase hydrophilicity of carbon support; (iii) it was demonstrated that semiconductive TiO_2 may be converted to conductive form [27]. It is shown that on Pd catalysts supported on hybrid TiO_2-C materials, prepared by solvothermal and slurry synthesis, excellent electrocatalytic activity for formic acid electrooxidation has been achieved. Results compare favorably with those obtained on Pd-supported catalysts on the commercial carbon black Vulcan.

2. Experimental

2.1. Materials

Furfural, chitosan of low molecular weight, saccharose and titanium (IV) isopropoxide were analytical grade and purchased from Sigma–Aldrich. Absolute ethanol was purchased by VWR and used as supplied. The metal precursor salt p.a. grade $PdCl_2$ was purchased from POCh. Formic acid solutions used for fuel cell measurements (3 M) and for palladium deposition were prepared from Chempur 80% p.a. formic acid. Vulcan XC-72 carbon black (Cabot Corp., USA) was used as received for comparative purpose.

2.2. Solvothermal synthesis of hybrid TiO_2-C supports

In a typical solvothermal synthesis [28], 1 g of furfural (Fu) and 1 g of titanium (IV) isopropoxide were dissolved in 18 mL of ethanol. The resulting solution was sealed into a glass vial inside a Teflon-lined autoclave, followed by solvothermal treatment at 175 °C for 16 h. The resulting brown solid was separated from the solution by filtration and washed several times with ethanol. The material was dried under static-air at 100 °C for 2 h and the resultant sample was denoted Fu-TiO_2-C. A similar procedure [29] was followed for the samples prepared from chitosan (Ch) and saccharose (Sac) and these solids were denoted Ch-TiO_2-C and Sac-TiO_2-C, respectively. The hybrid catalytic supports were obtained from the Fu-TiO_2-C, Ch-TiO_2-C and Sac-TiO_2-C precursors after calcinations under N_2 flow from ambient to 800 °C [23] and then maintaining this temperature for 5 h. The carbonized samples were denoted Fu-TiO_2-C-C, Ch-TiO_2-C-C and Sac-TiO_2-C-C, respectively.

2.3. Synthesis of Pd catalysts

An aqueous solution of metal precursor $PdCl_2$ (40 mM) was drop-wise added under stirring at 70 °C to 500 mL aqueous dispersion of 1 g of the hybrid supports containing four times excess of formic acid. After 2 h the catalysts were separated and washed 10 times with 500 mL of Millipore© water under stirring. After separation, the catalysts were dried at 80 °C in vacuum. The 20% Pd/Vulcan XC-72 reference catalyst was prepared according to the same procedure using as received carbon black Vulcan XC-72. The preparation and characterization of 10 wt.% Pd/SiO_2 catalyst used in a reference conductivity test is described elsewhere [30].

2.4. Characterization of supports and Pd-based catalysts

Textural characterization was performed by adsorption–desorption N_2 isotherms at 77 K. The full isotherms in the range of 4×10^{-3} to 84 kPa were measured in a Micromeritics ASAP-2020. Texture and pore size distributions (PSD) was discussed in terms of the surface area by BET method (S_{BET}), micropore volume ($V_{\mu pore}$) by t-plot method, mesopore volume (V_{meso}) by BJH adsorption cumulative pore volume of pores between 17 and 300 Å diameter, total pore volume (V_{tot}) by single point total pore volume of pores less than 2900 Å diameter at P/P_o close to 1, and pore diameter (D_{pore}) were obtained from the expression: $4V_{tot}/S_{BET}$. Hybrid supports were also characterized by powder X-ray diffraction (XRD). XRD patterns were recorded in the range of $2\theta = 2$–90° with a Cubix-PRO diffractometer from PANalytical with CuKα (1.54056) radiation and processed with the PW1877 program (Philips). Additional XRD experiments were performed on a Rigaku–Denki (Geigerflex) diffractometer using CuKα radiation (0.15418 nm) to characterize the palladium crystallite sizes in the catalysts.

Electrical resistance and sample height were measured at room temperature at compression pressures ranging from 60 to 150 atm. A sample of 0.05–0.01 g of the support or supported palladium catalyst was placed in a cylindrical aluminum dye fitted with PTFE tubing insert with inner diameter equal to 0.79 cm and compressed using hydraulic press between two metal plungers. The electrical resistance was measured by Agilent 34970A multimeter using the four point method. Because a constant mass of catalysts is used to form a catalyst layer, the results will be presented in the form of the product of specific conductivity and density:

$$\psi = \sigma \cdot \gamma = \frac{m}{R \cdot A^2} \quad (1)$$

where Ψ is the product of conductivity and density for the Pd catalysts [S g cm^{-4}]; σ is the conductivity of the sample, [S cm^{-1}]; γ is the density of the sample [g cm^{-3}]; m is the weight of the sample [g]; R is the measured resistance of the sample [Ω]; A is the surface area of the cross section surface of the sample (0.49 cm^2). The curves of the product (conductivity·density) as a function of pressure were plotted. The values of (conductivity·density) at pressure equal to 94.2 atm, which was the same as pressure applied to the catalyst layer in the fuel cell measurements conditions were determined from these curves.

Scanning-Transmission Electron Microscopy STEM studies were performed in a JEOL 2010F 200 kV microscope, with 0.19 nm spatial resolution. This instrument is equipped with a JEOL High Angle Annular Dark Field (HAADF) detector and an Oxford X-Max (80 mm^2) Silicon Drift X-Ray Energy Dispersive Spectroscopy (EDX) detector, enabling the acquisition of HAADF-STEM images and compositional analysis data (in spot mode or elemental mapping) using a 0.5 nm electron probe. Powder samples were prepared for the STEM studies by depositing a small amount of the powders directly onto Lacey-Carbon coated Cu grids.

2.5. Direct formic acid fuel cells measurements

Anodes for DFAFC were prepared from 25 mg of Pd catalyst and 5 wt.% Nafion Solution (Du Pont DE520) ultrasonicated with water for 30 min. The weight ratio of Pd catalyst, Nafion Solution and

water was 1:3:15, respectively. The resulting ink was drop casted by a Pasteur pipette on a 5 cm^2 carbon-cloth diffusion layer (carbon cloth B-1, designation A, Clean Fuel Cell Energy) which was followed by hot pressing (20 min at 0.8 kg cm^{-2}, 130 °C). The Pd loading on the anode was 0.5 mg cm^{-2}. For preparation of cathodes, 46 mg of 60 wt.% Pt/Vulcan catalyst (BASF Fuel Cells) and 5 wt.% Nafion Solution (Du Pont DE520) was ultrasonicated with water for 30 min. The weight ratio of Pd catalyst, Nafion Solution and water was 1:6:15, respectively. The resulting ink was drop casted by a Pasteur pipette on Teflon™-coated side of carbon-cloth layer (carbon cloth Designation B, 30% Wet Proffing; Basf Fuel Cell Co) for better water management. Cathode was hot pressed (0.8 kg cm^{-2}, 130 °C, 20 min). The Pt loading on the cathode was 4 mg cm^{-2}. The Nafion content in dry cathode was 33 wt.%. The fuel cell tests were conducted at room temperature and ambient pressure. The anode was fed with 3 M aqueous p.a. grade formic acid solution at a flow rate of 0.5 mL min^{-1} using peristaltic pump. The cathode was fed with O_2 at a flow rate of 1.0 L min^{-1}. The output voltage as a function of applied current were measured using home-made voltage controlled galvanostat and Agilent 34970A based data acquisition system.

2.6. The contact angles of water droplets on the anodes

A 20 μL droplett of water was placed on the surface of the anode prepared as described in Section 2.5. The contact angles of water droplets on the surface of the sample were measured by taking photos with Leica V-LUX 30 camera in the macro mode and analysis of the resulting photos.

3. Results and discussion

3.1. Characterization of supports

3.1.1. Texture

Table 1 shows a summary of textural properties of the hybrid supports. Fig. S1A in the supplementary material shows the N_2 adsorption–desorption isotherm of Fu-TiO_2-C. The results suggest that this hybrid material contains a mesoporous framework that can be classified as a type IV adsorption isotherm with an important hysteresis loop. This is in agreement with the moderate surface area of about 123 m^2 g^{-1} and with the mean pore diameter of about 7.7 nm (Table 1). By contrast, a type II adsorption isotherm with a very small and vertical hysteresis can be observed in Figs. S1B and S1C for Ch-TiO_2-C and Sac-TiO_2-C (supplementary material), respectively, which is attributed to aggregation of nanoparticles. Both isotherms correspond to mesoporous materials in agreement with the mean pore diameters ca. 33.5 nm and 18.5 nm, respectively, with a low surface area ca. 43 m^2 g^{-1} and 83 m^2 g^{-1} (Table 1) for Ch-TiO_2-C and Sac-TiO_2-C, respectively. Fig. S2A–S2C (supplementary material), show the N_2 adsorption isotherms of the support precursors Fu-TiO_2-C-C, Ch-TiO_2-C-C, and Sac-TiO_2-C-C, respectively after carbonization at 800 °C under N_2 flow and Table 1 summarize the textural parameter of these supports. A decrease in BET surface area (ca. 81 m^2 g^{-1}) and total pore volume (0.188 cm^3 g^{-1}) was found for Fu-TiO_2-C-C in comparison to Fu-TiO_2-C (123 m^2 g^{-1} and 0.236 cm^3 g^{-1}), while the mean pore diameter changed from ca. 7.7 nm to 9.3 nm. Table 1 also shows an increase of the BET surface area from 43 m^2 g^{-1} to 80 m^2 g^{-1}, a decrease in the total pore volume from 0.359 cm^3 g^{-1} to 0.243 cm^3 g^{-1} and a clear decrease of the mean pore diameter from ca. 33.5 nm to ca. 7.2 nm for Ch-TiO_2-C-C in comparison to non-carbonized Ch-TiO_2-C support. Also, an important increase in the BET surface area from 83 m^2 g^{-1} to 253 m^2 g^{-1}, with a remarkable increase in the total pore volume from 0.384 cm^3 g^{-1} to 0.661 cm^3 g^{-1} and also with a decrease from 18.5 nm to ca. 10.0 nm of the mean pore diameter was detected for Sac-TiO_2-C-C in comparison to Sac-TiO_2-C.

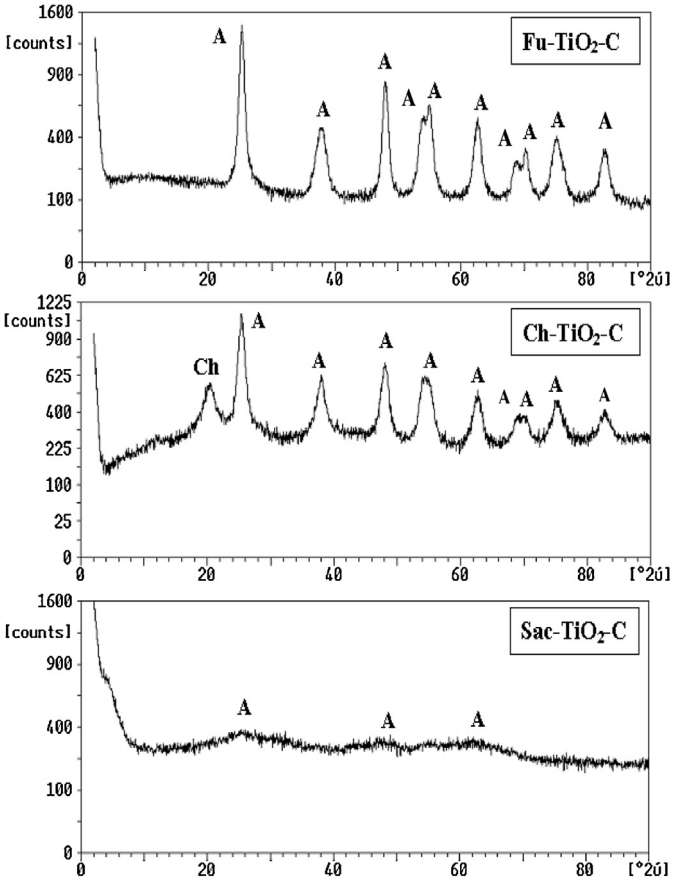

Fig. 1. XRD patterns of hybrid TiO_2-C supports. A: anatase; R: rutile; Ch: chitosan. Anatase peaks are marked as A (JCPDS 84-1285 or 83-2243), rutile phase peaks as R (JCPDS 86-0147).

For the case of the support prepared from furfural, the changes in the textural properties obtained after carbonization can be attributed to the oxygen group removal from the surface of the hybrid-material during carbonization and to the loss of carbon composition [31]. For the case of supports prepared from chitosan and saccharose, it can be seen an important enhance in the surface area indicating that activation of the carbon framework has occurred during carbonization, as reported elsewhere [32,33] for carbon foams obtained from the pyrolysis of saccharose. The apparent opposite behavior between furfural and chitosan and saccharose after the carbonization of supports was expected because furfural is a volatile liquid with a low flash point (62 °C) while the chitosan and saccharose have higher starting thermal degradation temperatures (200 °C) than the temperature of the solvothermal synthesis (175 °C) suggesting that an important contribution of carbon composition remains in the framework of these hybrid materials as suggest the remaining peak of chitosan and overlapping of saccharose detected by XRD patterns (Fig. 1). In consequence, the activation of pores during the carbonization at 800 °C under inert N_2 flow is expected in agreement with the increase of the surface area (Table 1). This is an important feature since it has been establish that the surface oxygen groups, which act as anchoring sites for metallic precursors as well as for metals, commonly determine the properties of carbon as a catalyst support [34,35].

Table 1
Textural properties of supports. Surface BET area (S_{BET}), micropore volume ($V_{\mu pore}$), mesopore volume (V_{meso}), total pore volume (V_{tot}), pore diameter (D_{pore}).

Support	S_{BET} ($m^2\ g^{-1}$)	$V_{\mu pore}$[a] ($cm^3\ g^{-1}$)	V_{meso}[b] ($cm^3\ g^{-1}$)	V_{tot}[c] ($cm^3\ g^{-1}$)	D_{pore}[d] (nm)
Fu-TiO_2-C	122.8	0.1016	0.1346	0.2362	7.7
Ch-TiO_2-C	42.8	0.0476	0.3110	0.3586	33.5
Sac-TiO_2-C	82.9	0.1134	0.2701	0.3835	18.5
Fu-TiO_2-C-C	80.6	0.1044	0.0838	0.1882	9.3
Ch-TiO_2-C-C	79.5	0.1121	0.1313	0.2434	7.2
Sac-TiO_2-C-C	253	0.1275	0.5339	0.6614	10.5

[a] Obtained by t-plot method.
[b] Obtained by BJH adsorption cumulative pore volume of pores between 17 and 300 Å diameter.
[c] Obtained by single point total pore volume of pores less than 2900 Å diameter at P/P_o close to 1.
[d] Obtained from expression: $4V_{tot}/S_{BET}$.

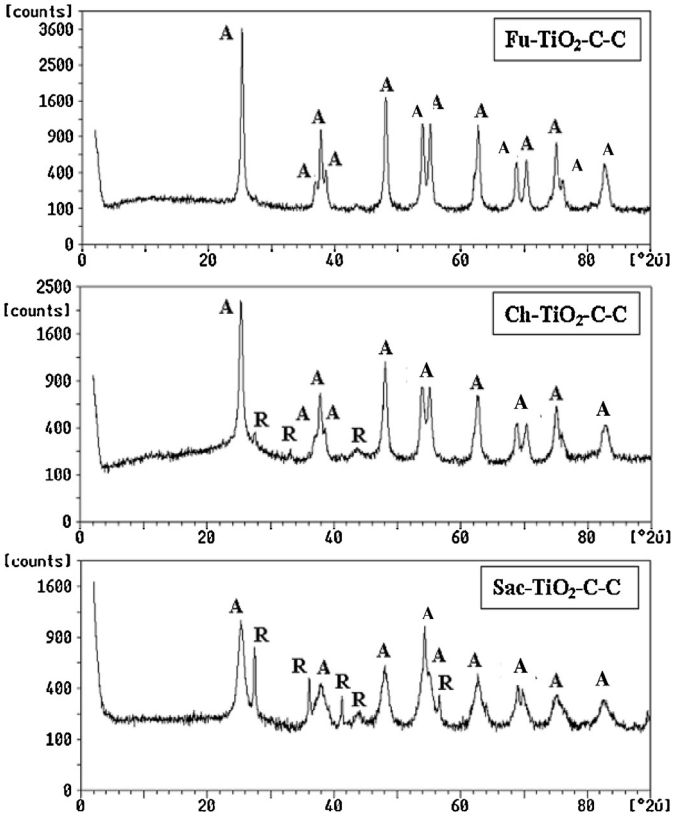

Fig. 2. XRD patterns of TiO_2-C supports after carbonization. A: anatase; R: rutile. Anatase peaks are marked as A (JCPDS 84-1285 or 83-2243), rutile phase peaks as R (JCPDS 86-0147).

3.1.2. XRD patterns

Fig. 1 shows the XRD patterns of Fu-TiO_2-C, Ch-TiO_2-C and Sac-TiO_2-C, while Fig. 2 presents the XRD patterns of the carbonized samples Fu-TiO_2-C-C, Ch-TiO_2-C-C and Sac-TiO_2-C-C. A summary of the TiO_2 crystalline phases detected is given in Table 2. It can be seen from Fig. 1 that TiO_2 mainly crystallizes as Anatase [28,36] with an Anatase:Rutile ratio of 100%:0% (Table 2) in both Fu-TiO_2-C and Ch-TiO_2-C. After carbonization (Fig. 2), the ratio Anatase:Rutile remains unchanged in Fu-TiO_2-C-C but changed to 80%:20% in Ch-TiO_2-C-C (Table 2). Also, it is clear that the crystallinity of TiO_2 in Fu-TiO_2-C-C and Ch-TiO_2-C-C clearly changes, suggesting the presence of larger TiO_2 crystallites. In the case of Sac-TiO_2-C, the XRD pattern (Fig. 1) showed that carbon fully overlaps the TiO_2 XRD peaks indicating the encapsulation of TiO_2 crystallites inside the carbon matrix. Fig. 2 shows an important contribution of the Rutile phase with an Anatase:Rutile ratio of about 60%:40% in the Sac-TiO_2-C-C support suggesting that a strong interaction between TiO_2 crystallites and C atoms has occurred during carbonization [28,37]. XRD pattern of Sac-TiO_2-C-C in Fig. 2 suggests TiO_2 is constituted by crystallites of smaller size than those composing Fu-TiO_2-C-C and Ch-TiO_2-C-C.

Table 2
Crystalline phase composition of TiO_2 in the different supports.

Solids	Anatase[a] (%)	Rutile[a] (%)
Fu-TiO_2-C	100	0
Ch-TiO_2-C	100	0
Sac-TiO_2-C	[b]	[b]
Fu-TiO_2-C-C	100	0
Ch-TiO_2-C-C	80	20
Sac-TiO_2-C-C	60	40

[a] Proportion obtained from the quantification of all anatase and rutile phases detected in the XRD patterns.
[b] Impossible to quantify but XRD pattern from Fig. 1 suggests anatase is the most important crystalline phase.

3.2. Characterization of the Pd/TiO_2-C catalysts

3.2.1. XRD patterns

X-ray powder diffractograms of the Pd/TiO_2-C catalysts in the 2Θ range between 20° and 90° is shown in Fig. 3. XRD pattern of 20 wt.% Pd supported catalysts shows that in addition to the presence of TiO_2 rutile and anatase, peaks at 2θ values of 40.2°, 46.5°, 68.2°, 82.0°, and 86.7°, respectively contains: 1 1 1, 2 0 0, 2 2 0, 3 1 1 and 2 2 2 of a Pd fcc system respectively are also presents. Pd crystallite sizes for the three catalysts supported on carbonized hybrid TiO_2-C and the reference Vulcan supported one are presented in Table 3. The pattern analysis with FITYK 0.9.0 program [38] using Pearson 7 function allowed calculations of Pd crystallite sizes in the presence of TiO_2 peaks. The crystallite sizes were determined from Scherrer equation by fit to the 1 1 1, 2 0 0 and 2 2 2 Pd fcc structure peaks:

$$d = \frac{0.9 \cdot \lambda}{\beta \cdot \cos\Theta} \quad (2)$$

where, λ, θ and β are the X-ray wavelength (0.15418 nm), Bragg diffraction angle, and the full width at half-maximum of the diffraction peak, respectively.

Pd crystallites sizes determined from 2 0 0 and 2 2 2 Pd fcc structure peaks are between 13 and 33 nm, while these determined from 1 1 1 peak are systematically higher (between 23 and 75 nm). This indicates that the Pd crystallites are longer along the 1 1 1 plane. In Table 3 are also shown the values of average Pd crystallites sizes ($d_{average}$) calculated from the 1 1 1, 2 0 0 and 2 2 2 Pd fcc structure peaks, and the fraction exposed (FE) of Pd crystallites is calculated from the equation (3):

$$FE = \frac{5.01 \cdot d_{at}}{d_{average}} \quad (3)$$

where d_{at} is atomic diameter for Pd equal to 0.274 nm [39].

Table 3
The average Pd particle sizes from XRD analysis.

Sample	2θ	FWHM	d (nm)	2θ	FWHM	d (nm)	2θ	FWHM	d (nm)	d_{ave} (nm)	FE[a]
Pd/Fu-TiO_2-C-C	40.10	0.46	23	46.64	0.73	13	86.60	0.74	19	18.3	0.075
Pd/Ch-TiO_2-C-C	40.17	0.36	46	46.72	0.52	22	86.69	0.65	33	33.7	0.041
Pd/Sac-TiO_2-C-C	40.15	0.33	75	46.70	0.50	20	86.71	0.61	33	42.7	0.032
Pd/Vulcan	40.02	0.56	15	46.56	0.77	11	86.55	0.80	14	13.3	0.103

[a] Fraction exposed was calculated from the equation FE = ($5.01 d_{at}/d_{ave}$) [39], being d_{at} the atomic diameter for Pd equal to 0.274 nm, and d_{ave} for Pd crystallites was calculated as an average value for three XRD peaks shown in Table 3.

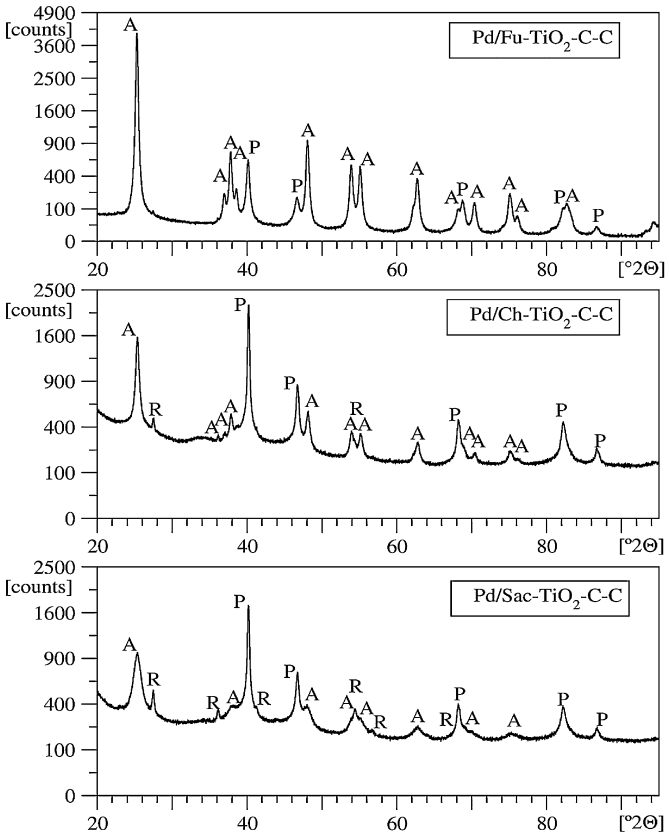

Fig. 3. XRD patterns of Pd/TiO_2-C catalysts. Anatase peaks are marked as A (JCPDS 84-1285 or 83-2243), rutile phase peaks as R (JCPDS 86-0147) and palladium peaks as P (JCPDS 46-1043).

3.2.2. *HAADF-STEM-EDX analysis of Pd-supported on carbonized hybrid materials*

Fig. 4A shows a HAADF-STEM image of the Fu-TiO_2-C-C sample. Compositional EDX analysis from Fig. 4A indicated that Pd/Fu-TiO_2-C-C catalyst is constituted at least by three different regions mainly composed by Ti and O (contrast 1 and 2) and by Pd nanoparticles supported in a hybrid region composed by Ti, O and C (contrast 3). Fig. 4B shows a higher magnification HAADF-STEM image from region 1. EDX spectra collected over outer part of the region showing the presence of Pd nanoparticles supported on TiO_2. As indicated the EDX analysis obtained showed that region 1 is mainly composed by Pd nanoparticles supported on TiO_2. Fig. 4C shows a higher magnification HAADF-STEM image from the region 2. The EDX analysis shows very different composition from different areas with Ti is the most important one. These findings are also applicable to the region 3 which showed Ti enriched areas. In general, when higher magnification images are addressed, the electron microscopy results confirm that Pd nanoparticles are preferentially supported on carbon, as shown in Fig. 4D. The Pd nanoparticles supported on the hybrid materials prepared from furfuran by solvothermal synthesis following carbonization (Fu-TiO_2-C-C) showed very different sizes from 2.3 up to 8.9 nm and from the analysis of about 100 particles a mean size of about 6.0 nm was found.

Fig. 5A shows a representative HAADF-STEM image of the Pd/Ch-TiO_2-C-C catalyst. It can be seen in Fig. 5B that contrary to the previous case, the Pd/Ch-TiO_2-C-C sample shows a morphological domain conformed by well dispersed small nanoparticles from 0.6 up to 7.8 nm with a mean size of 4.0 nm from 420 nanoparticles analyzed. EDX analysis confirms that the nanoparticles supported on the carbon support are constituted by Pd. Rigorous analysis was performed searching for TiO_2 nanoparticles but few Ti nanoparticles were detected. HAADF-STEM image of Fig. 5C shows the presence of few isolated TiO_2 crystals but no enriched Ti zones were found in the Pd/Ch-TiO_2-C-C samples in comparison with Pd/Fu-TiO_2-C-C (Fig. 4). The low proportion of TiO_2 nanoparticles could be the reason why in spite of Pd nanoparticles in Pd/Ch-TiO_2-C-C showed a better dispersion and a smaller mean size than Pd nanoparticles in the Pd/Fu-TiO_2-C-C sample. As we discussed below, contrary to the expected Pd/Fu-TiO_2-C-C showed two times higher maxima power developed from the formic acid electrocatalytic oxidation than that developed by Pd/Ch-TiO_2-C-C, indicating that the presence of hydrophilic TiO_2 phases is require for the enhancement in the catalytic activity.

For the Pd/Sac-TiO_2-C-C catalyst, Fig. 6 shows two different morphologies, a bulk composite (Fig. 6A) and microspheres (Fig. 6B). The two main features observed from Fig. 6 were the following. Pd nanoparticles are dispersed on carbon in the bulk material (Fig. 6A) and the presence of large Pd crystals even in the bulk and the microspheres (Fig. 6B). Fig. 6C shows a selected area of the Fig. 6A highlighted by a box over the HAADF-STEM while Fig. 6D–F, summarizes different EDX compositional analysis performed on the Pd/Sac-TiO_2-C-C catalyst. The chemical compositional for the EDX spectra show the occurrence of a very tiny Ti and O signals with the most dominant signal: Pd, relative to the nanoparticle, and C, from the support (Fig. 6D). However, both elemental distributions, either by the spectrum line mode (Fig. 6E) and/or the spectrum imaging mode (Fig. 6F), confirm that Pd nanoparticles are supported on carbon and as a general fact; no Ti signals were detected with the following exceptions. A small Ti signal detected below one of the largest Pd crystals (Fig. 6D) and TiO_2 crystallites detected in the microspheres shown in Fig. 7. It should be pointed out that TiO_2 is preferentially localized in the shell of the microspheres and also that carbon is presented in the core of the spheres, as it can be inferred from the elemental distribution maps included in Fig. 7. In other words, the above inference about the fact that Pd nanoparticles are preferentially supported on the carbon for the case of Pd/Ch-TiO_2-C-C seems to be confirmed in the case of Pd supported on Sac-TiO_2-C-C and this could be the consequence of lower maxima power detected during the electrocatalytic oxidation of formic acid in comparison Pd/Fu-TiO_2-C-C as discussed below.

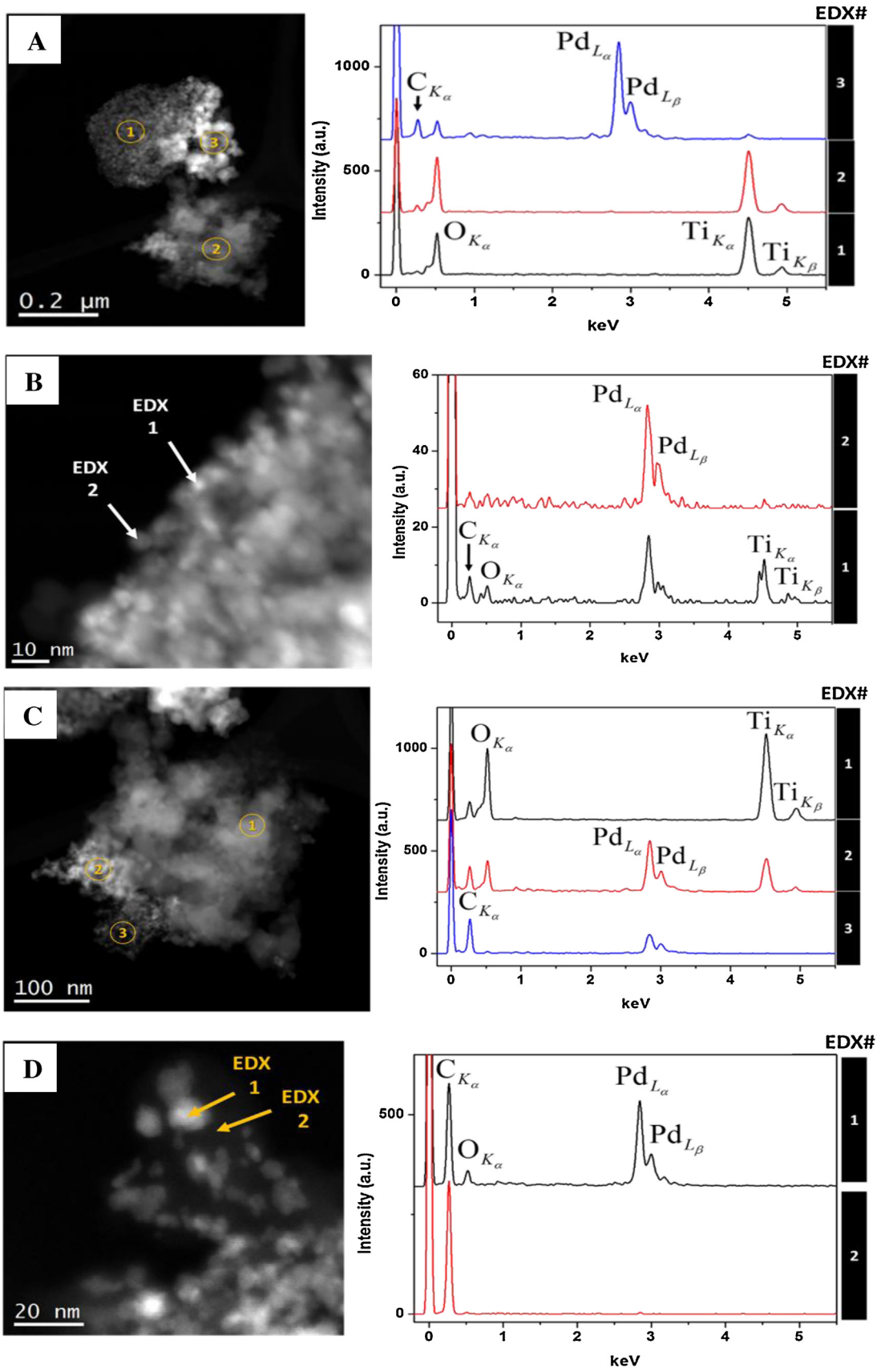

Fig. 4. (A): HAADF-STEM images and EDX spectra in three different regions of Pd/Fu-TiO_2-C-C. (B): Magnification of the region 1. (C): Magnification of the region 2. (D): Magnification of the region 2 mainly composed by carbon.

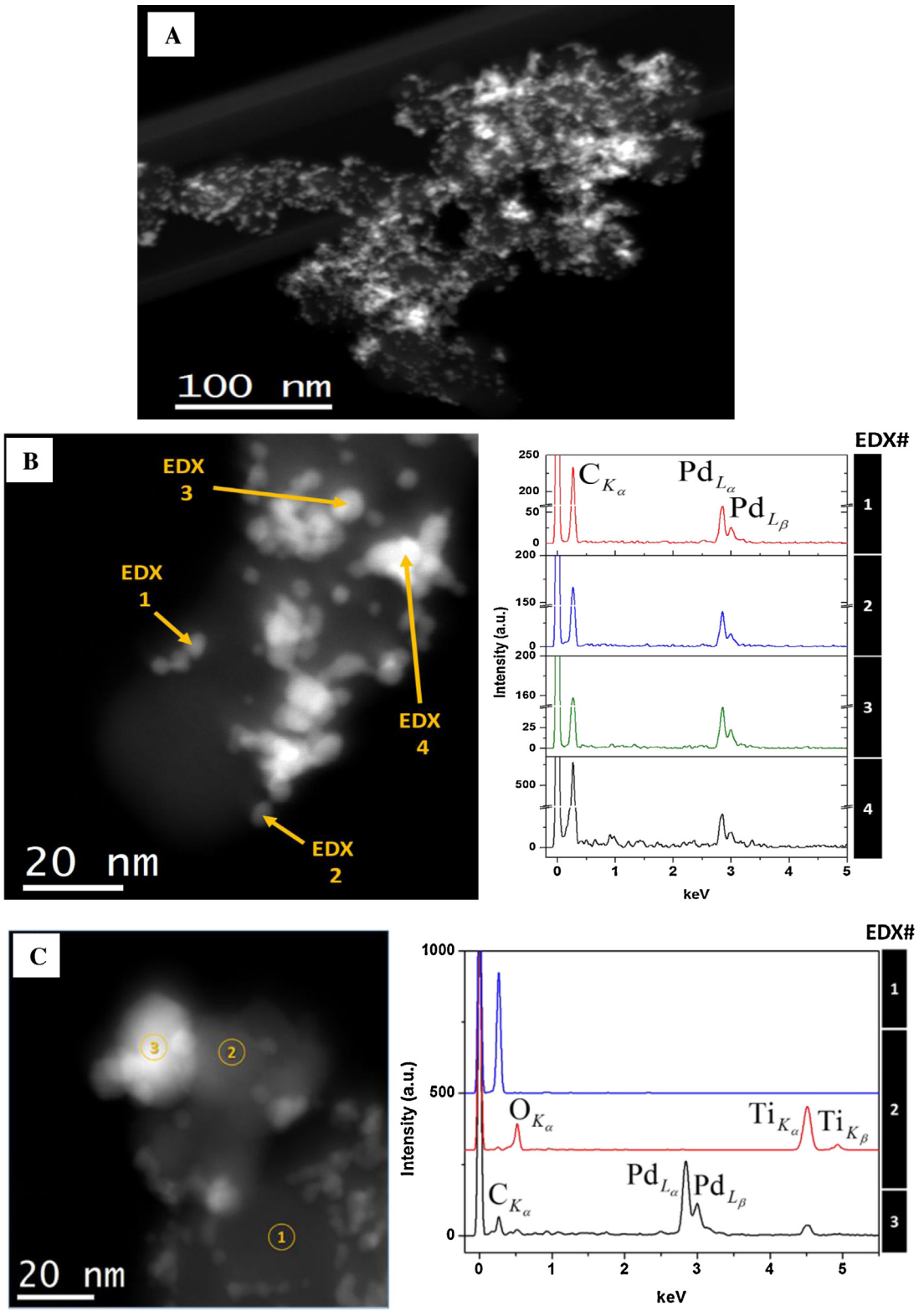

Fig. 5. (A): HAADF-STEM image of Pd/Ch-TiO_2-C-C. (B and C): HAADF-STEM image and corresponding EDX analysis of Pd/Ch-TiO_2-C-C.

3.2.3. Product of conductivity and density for the Pd catalysts

Electrons taking part in the formic acid electrooxidation have to be transferred from active sites in the anode catalysts layer to current collector. For this reason the catalysts supported on isolators such as SiO_2 are not used in fuel cells. It is known that rutile and anatase, the principal phases of titanium oxide, are semiconductors and their conductivity may not be sufficient for fuel cell application at high current densities. For this reason conductivities of TiO_2-C composites and Pd/TiO_2-C catalysts have been determined using DC measurements for samples compressed with the same pressure as that applied to the catalyst layer in the working DFAFC. The DC method has been chosen because high frequency resistance of fuel cell obtained from impedance spectroscopy contains also additional components from proton conductor in the membrane

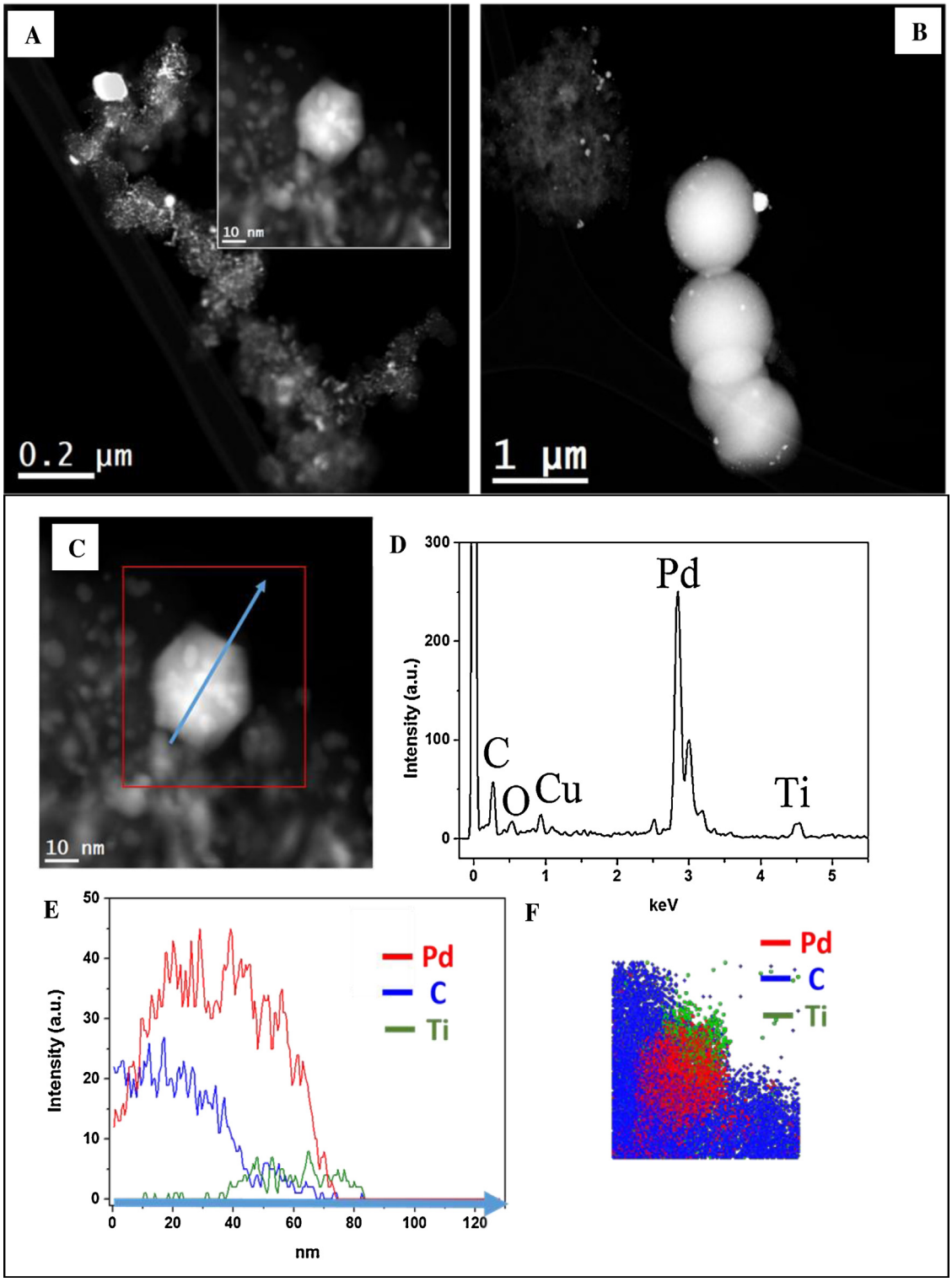

Fig. 6. (A–C): HAADF-STEM images of the Pd/Sac-TiO_2-C-C. (D): EDX spectra acquired from the selected box area. (E): Profile of element distribution through a particular arrowed direction. (F): Elemental distribution map in the box area.

and in the catalyst layers at anode and cathode, carbon clothes and current collectors. Therefore, the conductivity of the supported catalysts cannot be directly determined from impedance spectroscopy at fuel cell conditions.

Product of conductivity and density for the supports and the corresponding Pd supported catalysts are shown in Table 4. It can be seen that all hybrid TiO_2-C supports are poorly conductive. Their conductivities are several orders of magnitude lower than that for Vulcan XC-72. However, after palladium deposition, using formic acid as a reducer, the specific conductivities of the catalysts increased by 2–3 orders of magnitude. In order to explain the role of the presence of Pd on the surface of TiO_2-C composites in the observed increase of conductivity after Pd deposition, the conductivity of the Pd supported catalyst on a non-conductive support

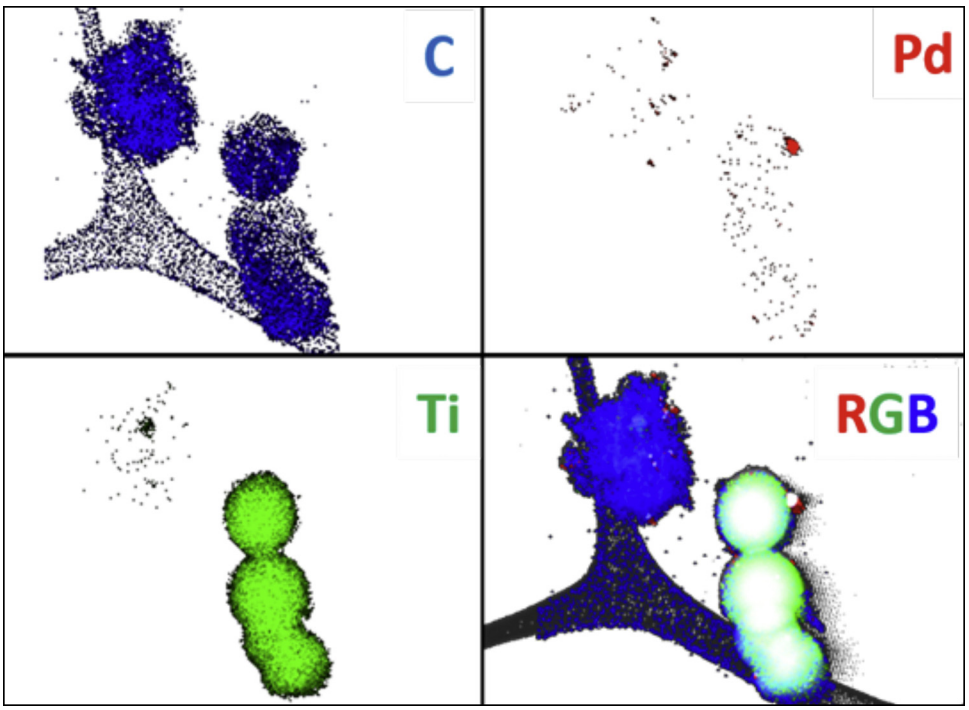

Fig. 7. Elemental distribution maps for C (blue), Pd (red) and Ti (green) and the composed red-green-blue (RGB) image for the three elements for Pd/Sac-TiO_2-C-C.(For interpretation of the references to color in this figure legend, the reader is referred to the web version of the article.)

Table 4
Power density maxima for the DFAFC with 20 wt.% Pd anodic catalysts synthesized on various supports, specific conductivities of respective supports and catalysts measured at 94.2 atm.

Support	Power maxima for Pd catalysts (mW/mg_{Pd})	Specific conductivity[a] for the supports ($S\,g\,cm^{-4}$)	Specific conductivity[a] for the Pd catalysts ($S\,g\,cm^{-4}$)
Fu-TiO_2-C-C	80.0	0.000383	0.342
Ch-TiO_2-C-C	39.9	0.00215	0.065
Sac-TiO_2-C-C	38.4	0.00049	0.32
Vulcan XC-72	24	2.75	2.42

[a] Estimated from Eq. (1)

(10 wt% Pd/SiO_2) was additionally measured. The estimated value of the product (conductivity·density) at pressure equal to 94.2 atm was more than seven orders lower than that found for Pd/TiO_2-C composites, what indicate that the percolation effects of Pd nanoparticles on the bulk electrical conductivity can be neglected. The lack of the conductivity of the Pd/SiO_2 catalyst can be explained by fact that Pd nanoparticles are fixed on nonconductive support and are electrically isolated. Therefore, the probability of the formation of conductive paths between Pd particles is very small. However, the observed increase of conductivity of TiO_2-C composites are in agreement with in situ ellipsometry studies of TiO_2 films on Ti subjected to the electrochemical reduction [27]. It was shown there that at cathodic potentials hydrogen incorporates into TiO_2 lattice increasing significantly conductivity of the TiO_2. Both forms of TiO_2 (rutile and anatase) are semiconductors of the bandgap of about 3 eV. The dissolved hydrogen atoms donate electrons to the conduction band according to reaction (4):

$$TiO_2 + H^+ + e^- = TiOOH. \quad (4)$$

The ellipsometry studies have demonstrated that the ratio of TiOOH to TiO_2 in the oxide film on Ti can be as high as 1:1 [27]. The same phenomenon may occur during catalysts preparation on carbonized hybrid TiO_2-C (Fu-TiO_2-C-C, Ch-TiO_2-C-C and Sac-TiO_2-C-C), because during palladium deposition by reduction of Pd^{2+} ions, TiO_2 acquires cathodic potential around 0 V vs. RHE, at which hydrogen atoms incorporate into TiO_2 lattice according to reaction (4). Such effect could explain the clearly much higher electrical conductivity experimentally observed on Pd/TiO_2-C catalysts than that on TiO_2-C hybrid supports (Table 4).

3.3. Direct formic acid fuel cells

The results of the catalyst testing in DFAFC are presented in Fig. 8. Power maxima for all the tested samples are shown in Table 4. All the catalysts supported on carbonized hybrid TiO_2-C, i.e. Fu-TiO_2-C-C, Ch-TiO_2-C-C and Sac-TiO_2-C-C, have higher activity per Pd mass unit than Pd supported on commercial Vulcan XC-72 carbon black commonly used as a support for FC catalysts. The Pd/Fu-TiO_2-C-C catalyst has three times higher activity per Pd mass unit than the catalyst prepared on a commercial Vulcan XC-72 carbon black, which will allow to reduce considerably the amount of expensive noble metal at the anode of DFAFC.

In order to learn how electronic conductivity of the anode catalyst layer influences the performance of DFAFC, data from Table 4 were used to calculate resistances of catalysts thin films with the dimensions of the catalyst layer used at the anode of DFAFC (anode geometric surface 5 cm^2, 2.5 mg catalyst per cm^2). These resistances represent the lower limit of the anode catalyst layer resistance because it does not take into account the presence of non-electronically conductive Nafion present in the layer. In Fig. 9 the calculated resistances are compared with resistances determined from the slope of voltage–current density relations (Fig. 8A)

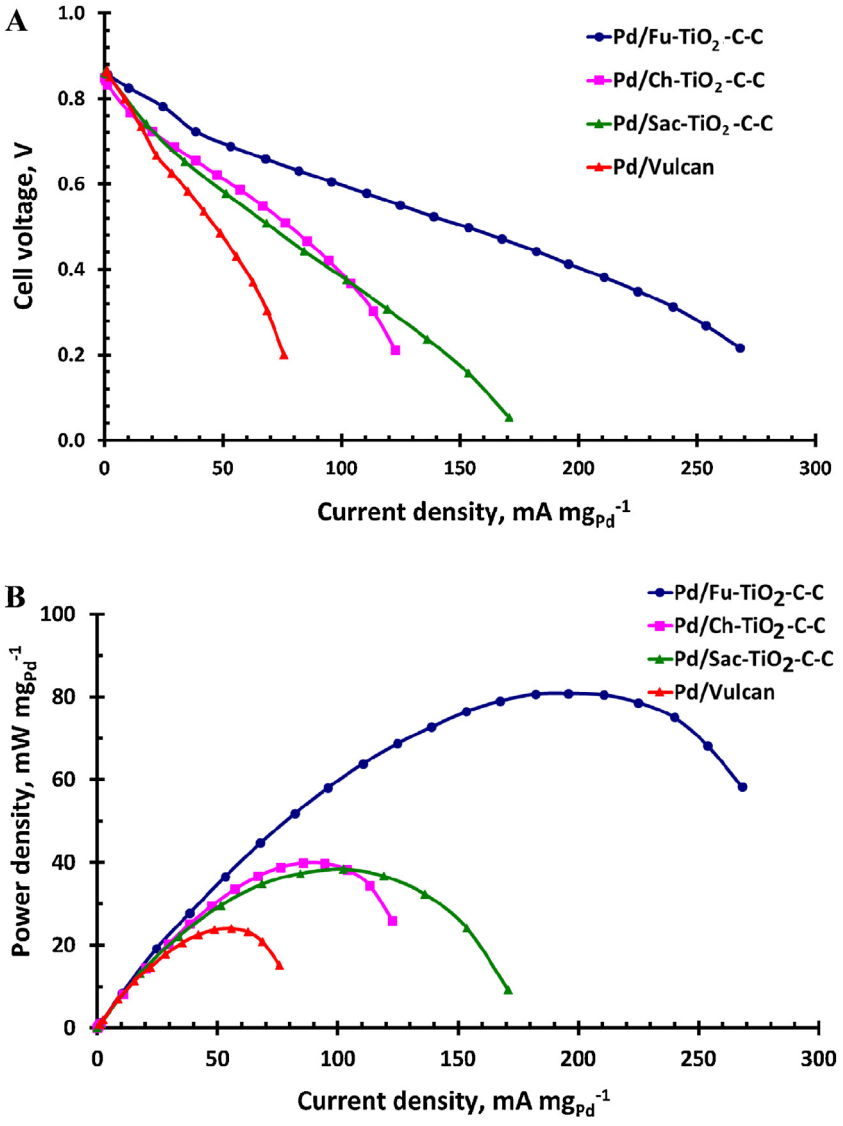

Fig. 8. Cell voltage (A), and power density as a function of current (B).

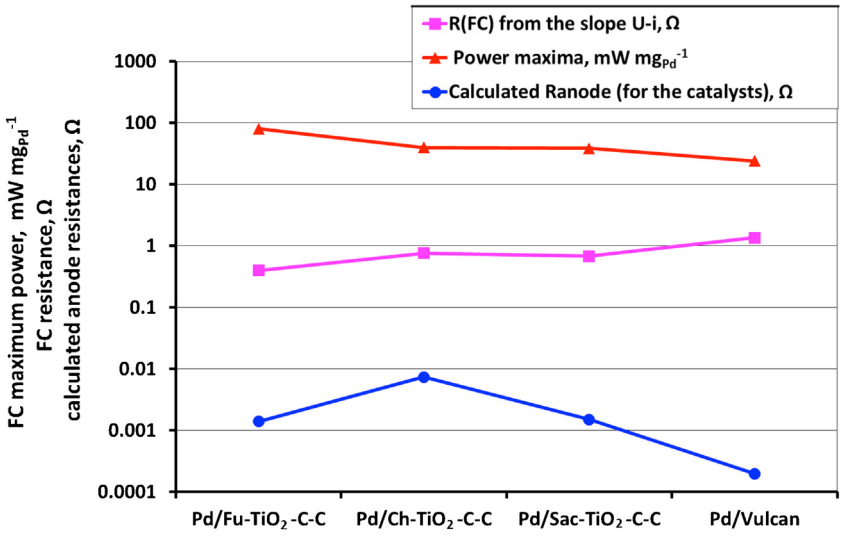

Fig. 9. Maxima power density of DFAFC for different anode catalysts and calculated anode resistances R(FC) of the layers made from the support and made from the catalysts (R_{anode}), using values of specific conductivity obtained experimentally at pressure of 94.2 atm.

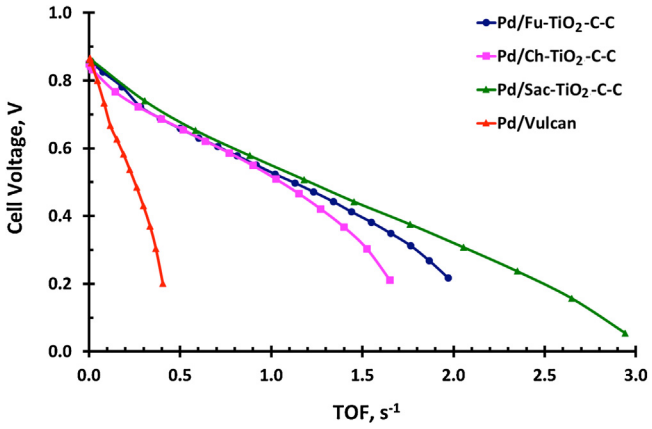

Fig. 10. Relation between cell voltage and turnover frequency for different catalysts.

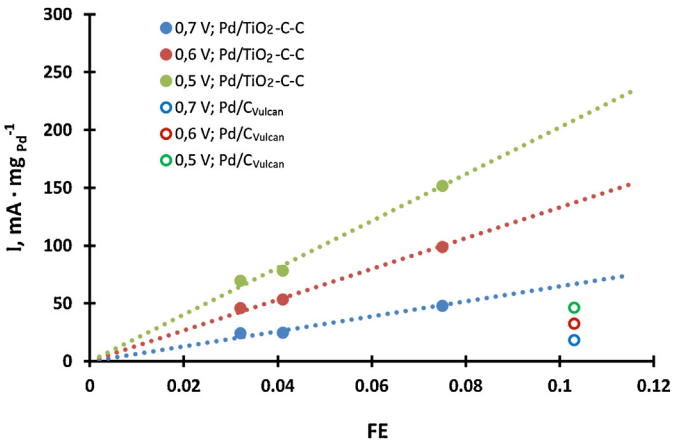

Fig. 11. The comparison of the effect of FE on specific current for Pd/TiO_2-C and Pd/C anode catalysts; Pd/TiO_2-C – filled circles; Pd/C – empty circles.

of the respective FC's. It can be seen from Fig. 9 that the calculated resistances are two to three orders of magnitude higher than the resistances obtained from the prepared anode, which indicates that electrical conductivity of the anode catalyst layer is not limiting the total resistance of FC and that the kinetics of formic acid electrooxidation and/or diffusion of formic acid to anode catalytic layer determines the total resistance and the fuel cell performance. In order to learn how the size of Pd crystallites influence the rate of formic acid electro-oxidation calculated per one atom of Pd on the surface of Pd crystallites so-called turn over frequency (TOF) was calculated using FE shown in Table 3, and results of these calculation are shown in Fig. 10.

It can be seen from Fig. 10 that the rate of electrooxidation of formic acid, for all Pd/TiO_2-C catalysts, for TOF below 1 s^{-1} is independent of the size of crystallites nor surface structure and this process may be designated as "structure-insensitive" [40,41]. It is believed that for this type of reaction rate limiting step takes place at an active center consisting of single surface atom on the metal crystallite [42–44]. However, at the region of high current densities, TOF is no longer independent of FE of Pd. This is because TOF's were calculated assuming that all the surface Pd atoms in the anode layer are electrochemically available and at the region of high current densities only part of the surface Pd atoms participate in electrooxidation due to formic acid transport limitations or blocking of access of formic acid to active centers by CO_2 bubbles [45]. These results suggest that all surface Pd atoms are electrochemically available for Pd/TiO_2-C catalysts in the low range of reaction rate (TOF below 1 s^{-1}). In turn, TOF for Pd/Vulcan catalyst is about five times lower than for Pd/TiO_2-C catalysts what may indicate that only small part of active sites are available for this catalyst. From contact angle measurements on tested anodes it was found that hydrophilicity of all the Pd/TiO_2-C catalysts is higher than that of Pd/Vulcan catalyst (Table 5). It suggests that higher activity of Pd/TiO_2-C catalysts than Pd/Vulcan can be attributed to their higher hydrophilicity, which prevents formation of CO_2 bubbles blocking access of formic acid to the surface Pd atoms in the anode catalyst layer [45]. Rapid decrease in cell voltage for TOF > 1 s^{-1} (Fig. 10) suggests, that the rate of the transport of reactants begins to limit the rate of the whole anodic process. These results are in agreement with the previous studies [25,26], were it was shown that the hydrophilicity of the anode catalytic layer of the DFAFC affects considerably the rate of HCOOH penetration into the catalyst layer, and so, activity of the anode. It was demonstrated, that optimum hydrophilicity depends on the temperature and formic acid concentration. In the case of low concentration of formic acid, used in our studies, very hydrophilic diffusion structure ensures the best operation of the anode of the DFAFC.

The higher hydrophilicity of the Pd/TiO_2-C catalysts may be due to the presence of hydrophilic TiO_2 oxide in the developed TiO_2-C composites. For the low rates of electrooxidation of formic acid these curves overlap (Fig. 10), which indicates that diffusion of the acid in Pd/TiO_2-C catalysts does not affect the rate of the process. In contrast, much lower activity of the Pd/Vulcan catalyst may be due to its higher hydrophobicity, limiting the penetration rate of formic acid into the catalytic layer at the anode in the whole range of currents and reduces the electrochemically available surface area of Pd in the catalyst layer.

At low range of TOF (below 1 s^{-1}) when TOF is independent on Pd particle sizes the reaction rate per mass unit of Pd, and so the specific current, should be proportional to FE of Pd crystallites, what is really observed in Fig. 11 for Pd/TiO_2-C catalysts. As it follows from this figure, the activity of this type of catalyst is high in spite of that FE is relatively low (below 0.08). Therefore, the activity can be increased considerably by increasing of FE of the Pd crystallites. This can be achieved by: (i) optimization of preparation methodology, (ii) increasing fraction of mesopores of sizes larger than these of Pd crystallites (Table 1), which would increase the degree of utilization of the inner surface of the support available for Pd crystallites of the size between 2 and 10 nm.

This suggestion can be inferred from the comparison between the values of the mean pore sizes of the supports (Table 1) and power density maxima for the DFAFC reaction (Table 4). It can be seen that the higher the $V_{\mu pore}/V_{tot}$ ratio of the support (Table 1) the higher the catalytic activity (Table 4), being the maxima observed for the support prepared from furfural with about 56% micropore volume. However, further studies with more supports and with a wider range in the mean pore sizes should be done to establish a proper relationship between both parameters.

As a final remark, XRD plots and mainly the HAADF-STEM-EDX analysis have permitted the understanding of the interaction between Pd nanoparticles and the components of the present hybrid materials. STEM images and EDX suggest important differences in the catalytic activity of the different catalysts. Pd

Table 5
Contact angles of water droplets on the anodes.

Catalyst support	Average contact angle (°)	Standard error (°)
Vulcan XC-72	137.0	1.6
Fu-TiO_2-C-C	126.4	3.1
Ch-TiO_2-C-C	126.9	2.0
Sac-TiO_2-C-C	125.0	1.9

nanoparticles require not only a high dispersion on supports but also an important contribution from hydrophilic TiO_2 which is able to diffuse from the hybrid TiO_2-C framework as suggest the EDX analysis showed in the Figs. 4–7. This interaction between Pd and TiO_2-C hybrid support explains the high catalytic activity up to three times higher for Pd/Fu-TiO_2-C-C than Pd-supported catalysts on the commercial carbon black Vulcan. In addition, in a recent paper from our group [46] we have shown that the oxygen functional groups on carbon framework in hybrid materials are able to interact with TiO_2 preferentially with the anatase crystalline phases than with the rutile phase due to a more oxygen vacancy in the anatase. The higher catalytic activity showed in the present work was obtained on Pd/Fu-TiO_2-C-C characterized by the higher anatase proportion in the TiO_2 framework (Table 2).

4. Conclusions

All of the raw hybrid TiO_2-C supports have conductivities several orders of magnitude lower than that for Vulcan XC-72. After palladium catalysts preparation on Fu-TiO_2-C-C, Ch-TiO_2-C-C and Sac-TiO_2-C-C supports, the conductivities of the resulting Pd/TiO_2-C catalysts increase to such a level, that they do not limit the fuel cell performance. The activity per Pd mass unit of the Pd/Fu-TiO_2-C-C catalyst is about three times higher than that of Pd/Vulcan XC-72 although the FE of the Pd/Vulcan is the highest. The rate of electrooxidation of formic acid on Pd/TiO_2-C catalysts, calculated per one surface Pd atom (TOF), is for TOF < 1 s^{-1} independent of Pd particle size and morphology of the supports. Beneficial properties of Pd/TiO_2-C can be explained by both: their high hydrophilicity and sufficiently high electrical conductivity. Taking into account that FE of Pd particles were relatively low (below 0.08), there is still a considerable margin for improving the catalyst performance by decreasing palladium particle size, therefore, hybrid inorganic/organic materials presented here are potential supports for the direct formic acid fuel cell with Pd-based catalysts.

Acknowledgments

J. Matos thanks to Prof. Avelino Corma (ITQ-UPV, Spain) for the facilities to perform the synthesis and part of the characterization of the hybrid supports. A. Borodzinski thanks NCBiR for financial support through the project PBS1/A5/15/2012. The authors are grateful to M. Bonarowska for providing the Pd/SiO_2 catalyst for reference conductivity measurements.

Appendix A. Supplementary data

Supplementary data associated with this article can be found, in the online version, at http://dx.doi.org/10.1016/j.apcatb.2014.07.063.

References

[1] E. Casado-Rivera, D.J. Volpe, L. Aiden, C. Lind, C. Downie, T. Vázquez-Alvarez, A.C.D. Angelo, F.J. DiSalvo, H.D. Abruña, J. Am. Chem. Soc. 126 (2004) 4043–4049.
[2] J. Cao, L. Song, J. Tang, J. Xu, W. Wanga, Z. Chen, Appl. Surf. Sci. 274 (2013) 138–143.
[3] J. Chen, Y. Li, S. Liu, G. Wang, J. Tian, C. Jiang, S. Zhu, R. Wang, Appl. Surf. Sci. 287 (2013) 457–460.
[4] W.L. Qu, Z.B. Wang, X.L. Sui, D.M. Gu, G.P. Yin, J. Fuel Cells 13 (2013) 149–157.
[5] K.Y. Chen, P.K. Chen, A.C.C. Tseung, J. Electrochem. Soc. 142 (1995) L54–L56.
[6] A.C.C. Tseung, K.Y. Chen, Catal. Today 38 (1997) 439–443.
[7] E. Antolini, F. Cardellini, J. Alloys Compd. 315 (2001) 118–122.
[8] E. Antolini, Mater. Chem. Phys. 78 (2003) 563–573.
[9] N. Rajalakshmi, H. Ryu, M.M. Shaijumon, S. Ramaprabhu, J. Power Sources 140 (2005) 250–257.
[10] Z. Zhang, Y. Huang, J. Ge, C. Liu, T. Lu, W. Xing, Electrochem. Commun. 10 (2008) 1113–1136.
[11] C.H. Chen, W.J. Liou, H.M. Lin, S.H. Wu, A. Borodzinski, L. Stobinski, P. Kedzierzawski, Fuel Cells 10 (2010) 227–233.
[12] L. Lai, G. Huang, X. Wang, J. Weng, Carbon 49 (2011) 1581–1587.
[13] C. Rice, R.I. Ha, R.I. Masel, P. Waszczuk, A. Wieckowski, T. Barnard, J. Power Sources 111 (2002) 83–89.
[14] Y.M. Zhu, S.H. Ha, R.I. Masel, J. Power Sources 130 (2004) 8–14.
[15] S. Ha, Y. Zhu, R.I. Masel, Fuel Cells 4 (2004) 337–343.
[16] R. Larsen, S. Ha, J. Zakzeski, R.I. Masel, J. Power Sources 157 (2006) 78–84.
[17] X. Xu, P.G. Pickup, J. Power Sources 182 (2008) 124–132.
[18] L. Zhang, T. Lu, J. Bao, Y. Tang, C. Li, Electrochem. Commun. 8 (2006) 1625–1627.
[19] C.M. Miesse, W.S. Jung, K.J. Jeong, J.K. Lee, J. Lee, J. Han, S.P. Yoon, S.W. Nam, T.H. Lim, S.A. Hong, J. Power Sources 162 (2006) 532–540.
[20] W.S. Yung, J. Han, S. Ha, J. Power Sources 173 (2007) 53–59.
[21] X. Wang, J.M. Hu, I.M. Hsing, J. Electroanal. Chem. 562 (2004) 73–80.
[22] G. Girishkumar, M. Rettker, R. Underhile, D. Binz, K. Vinodgopal, P. McGinn, P. Kamat, Langmuir 21 (2005) 8487–8494.
[23] J. Matos, M. Rosales, R. Demir-Cakan, M.M. Titirici, Appl. Catal. A: Gen. 386 (2010) 140–146.
[24] J. Shim, C.R. Lee, H.K. Lee, J.S. Lee, E.J. Cairns, J. Power Sources 102 (2001) 172–177.
[25] S. Uhm, J.K. Lee, S.T. Chung, J. Lee, J. Ind. Eng. Chem. 14 (2008) 493–498.
[26] S. Uhm, Y. Kwon, S.T. Chung, J. Lee, Electrochim. Acta 53 (2008) 5162–5168.
[27] C.K. Dyer, J.S.L. Leach, J. Electrochem. Soc. 125 (1978) 23–29.
[28] J. Matos, A. García, L. Zhao, M.M. Titirici, Appl. Catal. A: Gen. 390 (2010) 175–182.
[29] J. Matos, P. Atienzar, H. García, J.C. Hernández-Garrido, Carbon 53 (2013) 169–181.
[30] M. Bonarowska, W. Juszczyk, Z. Karpiński, J. Catal. 301 (2013) 112–115.
[31] M. Inagaki, K.C. Park, M. Endo, New Carbon Mater. 25 (2010) 409–420.
[32] J. Matos, M. Labady, A. Albornoz, J. Laine, J.L. Brito, J. Mater. Sci. 39 (2004) 3705–3716.
[33] J. Matos, M. Labady, A. Albornoz, J. Laine, J.L. Brito, J. Mol. Catal. A: Chem. 228 (2005) 189–194.
[34] F. Coloma, A. Sepulveda-Escribano, J.L.G. Fierro, F. Rodriguez-Reinoso, Appl. Catal. A: Gen. 150 (1997) 165–183.
[35] J. Matos, J. Laine, Appl. Catal. A: Gen. 241 (2003) 25–38.
[36] Y. Wang, G. Zhou, T. Li, W. Qiao, Y. Li, Catal. Commun. 10 (2009) 412–415.
[37] R. Koc, J.S. Folmer, J. Am. Ceram. Soc. 80 (1997) 952–956.
[38] FITYK program home page: http://www.unipress.waw.pl/fityk/
[39] A. Borodzinski, M. Bonarowska, Langmuir 13 (1997) 5613–5620.
[40] G.C. Bond, Surf. Sci. 156 (1985) 966–981.
[41] M. Boudart, Adv. Catal. 20 (1969) 153–166.
[42] M. Che, C.O. Bennett, Adv. Catal. 36 (1989) 55–172.
[43] A. Borodziński, G.C. Bond, Catal. Rev. Sci. Eng. 50 (2008) 379–469.
[44] V. Ponec, Adv. Catal. 32 (1983) 149–214.
[45] A. Mikołajczuk, A. Borodzinski, P. Kedzierzawski, L. Stobinski, B. Mierzwa, R. Dziura, Appl. Surf. Sci. 257 (2011) 8211–8214.
[46] J. Matos, R. Montaña, E. Rivero, A. Escudero, D. Uzcategui, Water Sci. Technol. 69 (2014) 2184–2190.